Molecular field and Monte Carlo study for the mixed-spin axial next-nearest-neighbor Ising model

T. Kasama,[1] Y. Muraoka,[2] and T. Idogaki[1]
[1]*Department of Applied Quantum Physics, Kyushu University, Fukuoka 812-8581, Japan*
[2]*Department of General Education, Ariake National College of Technology, Omuta, Fukuoka 836-8585, Japan*
(Received 20 July 2005; revised manuscript received 3 February 2006; published 7 June 2006)

The mixed-spin axial next-nearest-neighbor Ising model, in which spin $S=1$ and spin $\mu=1/2$ ferromagnetic layers are stacked along the c axis alternately, is studied by using the molecular field approximation (MFA) and Monte Carlo (MC) simulation. The finite-temperature magnetic phase diagram obtained by the MFA shows a partially disordered phase (PDP) and the crossover behavior between two PDPs of periodicity 4, one including paramagnetic S spins and the other including paramagnetic μ spins. The appearance of the PDP and the crossover behavior predicted by the MFA are confirmed by MC simulation. The crossover behavior of the PDP is a coupled effect between the mixed spin and the frustration of the exchange interactions.

DOI: 10.1103/PhysRevB.73.214411 PACS number(s): 75.10.Hk, 05.50.+q, 75.30.Kz

I. INTRODUCTION

In recent years, both experimental and theoretical efforts toward understanding of the thermodynamic behavior of mixed-spin systems and frustrated magnets have been made. A molecular-based ferrimagnet is one prime example of such mixed-spin systems. Kaneyoshi and co-workers studied ferrimagnetic binary alloys, in which magnetic ions with different spin values S_A and S_B are randomly distributed. The results of the molecular field approximation (MFA) for various values of S_A and S_B revealed the existence of the multicompensation points, at which the total magnetization of the system vanishes below the Néel temperature.[1] Ohkoshi *et al.* first experimentally observed the appearance of two compensation points in the quaternary alloy Prussian Blue analog[2] and theoretically explained those features in terms of the molecular field approximation.[2]

Recently, Bobak *et al.* have claimed that even the case of the ternary mixed-spin Ising model has the possibility of giving two compensation points by detailed MFA calculation based on the structure of the Prussian Blue analog.[3] These unexpected features, in the sense that Néel's pioneering works in ferrimagnetism expected only one compensation point, of multicomponent alloys give the motivation for analyzing the mixed-spin systems in detail.

On the other hand, the antiferromagnetic triangular lattice Ising model is a typical example of frustrated systems. As is well known, this model with only the nearest-neighbor (NN) antiferromagnetic exchange interaction has no long-range-ordered state,[4] but with the introduction of the next-nearest-neighbor (NNN) ferromagnetic exchange interaction it exhibits interesting ordering such as a partially disordered antiferromagnetic phase, in which two-thirds of the spins are antiferromagnetically ordered while the other remains incoherent.[5,6] Using these results, Mekata and Adachi explained the successive phase transitions observed in $CsCoCl_3$.[7] On the other hand, without the introduction of the NNN ferromagnetic interactions mentioned above, it has been reported that the change of the spin value S leads to long-range ordering in the antiferromagnetic triangular lattice.[8] This fact suggests the importance of the role of the spin magnitude in frustrated systems.

The axial next-nearest-neighbor Ising (ANNNI) model is also a good example of a frustrated anisotropic spin system with competing interactions. Owing to the competition between the NN and NNN interlayer interactions along the c axis, its phase diagram calculated by the MFA qualitatively reproduced the successive phase transitions of the spatially modulated spin configurations[9] found in CeSb.[10] However, the usual simple ANNNI model could not reproduce the partially disordered phase (PDP), in which spin-ordered and spin-disordered sublattices coexist. In previous reports, we proposed an extended ANNNI model, in which spin layers with weak intralayer interaction and those with a strong one are alternately stacked along the c axis in addition to the competition of the NN and NNN interlayer interactions.[11] A MFA study of this intralayer-interaction-alternating ANNNI model showed that the PDP can appear in the intermediate temperature region.[11] Furthermore, we confirmed the stability of the PDP by later Monte Carlo (MC) simulation.[11,12]

From these studies, we expect that, in frustrated spin systems, modifications of the interaction strength and/or the spin magnitude play very important roles and cause various interesting phenomena, e.g., the appearance of the PDP and its related features. Those expectations led us to study the mixed-spin effects in a frustrated system.

In this paper, by using the MFA and MC simulation, we discuss the mixed-spin ANNNI model (Fig. 1), in which ferromagnetic layers composed of spins S and μ (hereafter, we call these layers the S layer and the μ layer, respectively) are stacked alternately. This system is described by

$$\mathcal{H} = -J_0 S^2 \sum_{\langle ij \rangle} S_i S_j - J_0' \mu^2 \sum_{\langle ij \rangle} \mu_i \mu_j - J_1 S \mu \sum_{\langle ij \rangle} S_i \mu_j - J_2 S^2 \sum_{\langle ij \rangle} S_i S_j - J_2' \mu^2 \sum_{\langle ij \rangle} \mu_i \mu_j. \quad (1)$$

In Eq. (1), J_0 and J_0' represent the ferromagnetic intralayer interactions for the S and μ layers, respectively. J_1 is the NN ferromagnetic interlayer interaction and J_2 (J_2') is the NNN

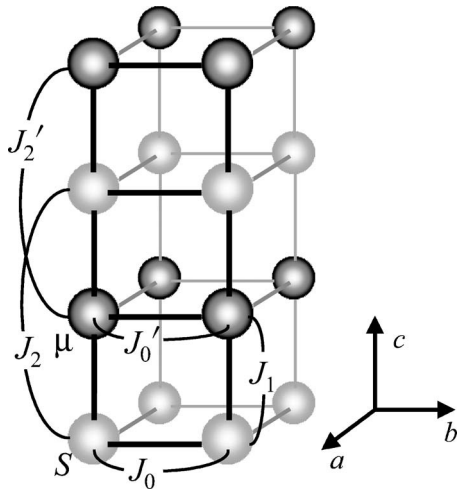

FIG. 1. Mixed-spin ANNNI model. It is composed of two kinds of alternately stacked $S=1$ (light spheres) and $\mu=1/2$ (dark spheres) ferromagnetic layers.

antiferromagnetic interlayer interaction between S layers (μ layers). S_i (μ_j) is the spin variable, which is normalized by its spin magnitude, sitting on the ith (jth) site. In the present study, we assume $S=1$ and $\mu=1/2$, and then S_i (μ_j) takes one of $\pm 1, 0$ (± 1) spin states. The summations run over the spin pairs with respect to each interaction.

The arrangement of this paper is as follows. In Sec. II, we show the expressions of the layer magnetizations and the free energy based on the MFA, and explain the finite-temperature magnetic phase diagrams obtained for various strengths of the exchange interactions. In Sec. III, by using MC simulation, we look for the existence of the PDP and its relevant phenomena suggested by the MFA in Sec II. Finally, in Sec IV, we conclude and discuss the spin-mixing effects on the ANNNI model.

II. MOLECULAR FIELD APPROXIMATION

A. Layer magnetizations and free energy

For the ferromagnetic intralayer interactions, it is believed that all spins within the same layer take the same thermal average. Imposing periodic boundary conditions and using a site-dependent MFA, Eq. (1) can be reduced to the following chain Hamiltonian:

$$\mathcal{H}_{\mathrm{MF}} = -J_1 S\mu \sum_{i=1}^{N/2} \left((S_{2i-1}H_{2i-1} + \mu_{2i}H_{2i}) - \frac{1}{2}(\langle S_{2i-1}\rangle H_{2i-1} + \langle \mu_{2i}\rangle H_{2i}) \right), \tag{2}$$

where

$$H_{2i-1} = 4\alpha_S \langle S_{2i-1}\rangle + (\langle \mu_{2i-2}\rangle + \langle \mu_{2i}\rangle) + \kappa_S(\langle S_{2i-3}\rangle + \langle S_{2i+1}\rangle), \tag{3}$$

$$H_{2i} = 4\alpha_\mu \langle \mu_{2i}\rangle + (\langle S_{2i-1}\rangle + \langle S_{2i+1}\rangle) + \kappa_\mu(\langle \mu_{2i-2}\rangle + \langle \mu_{2i+2}\rangle). \tag{4}$$

In Eqs. (2)–(4), S_{2i-1}, μ_{2i}, $\langle S_{2i-1}\rangle$, and $\langle \mu_{2i}\rangle$ denote the spin S on the $(2i-1)$th layer, the spin μ on the $2i$th layer, and their thermal averages, respectively. Hereafter, we use the following notations for the ratio of the exchange interactions normalized by the spin magnitudes:

$$\alpha_S = \frac{J_0 S^2}{J_1 S\mu}, \quad \alpha_\mu = \frac{J_0' \mu^2}{J_1 S\mu}, \quad \kappa_S = \frac{J_2 S^2}{J_1 S\mu}, \quad \kappa_\mu = \frac{J_2' \mu^2}{J_1 S\mu}. \tag{5}$$

From Eqs. (2)–(5), for the present case of $S=1$ and $\mu=1/2$, the thermal averages of the layer magnetizations per spin are given by

$$\langle S_{2i-1}\rangle = \frac{2\sinh KH_{2i-1}}{1+2\cosh KH_{2i-1}}, \tag{6}$$

$$\langle \mu_{2i}\rangle = \tanh KH_{2i}, \tag{7}$$

and the free energy per spin is given by

$$\frac{F}{J_1 S\mu} = \frac{1}{NK}\sum_{i=1}^{N/2} \left(\frac{K}{2}(\langle S_{2i-1}\rangle H_{2i-1} + \langle \mu_{2i}\rangle H_{2i}) - \ln(1+2\cosh KH_{2i-1})(2\cosh KH_{2i}) \right), \tag{8}$$

where

$$K = \frac{J_1 S\mu}{k_{\mathrm{B}}T}. \tag{9}$$

To determine probable configurations of spins, the simultaneous equations for the spin layers up to $N=16$ are self-consistently solved by means of the iteration. The most stable spin structure is determined so as to minimize the free energy of Eq. (8).

In order to evaluate the wave-number-dependent phase transition temperature, here we introduce a site-dependent fictitious field h_j. In the paramagnetic state, the $\langle S_{2i-1}\rangle$ and $\langle \mu_{2i}\rangle$ induced by the site-dependent external field h_j are calculated from Eqs. (6) and (7), and are given by neglecting higher orders of H_{2i-1}, H_{2i}, and h_j as follows:

$$\langle S_{2i-1}\rangle \approx \frac{2}{3}K(H_{2i-1} + g\mu_{\mathrm{B}}h_{2i-1}), \tag{10}$$

$$\langle \mu_{2i}\rangle \approx K(H_{2i} + g\mu_{\mathrm{B}}h_{2i}), \tag{11}$$

where g and μ_{B} denote the g factor and Bohr magneton, respectively. Now, we introduce the Fourier components of $\langle S_{2i-1}\rangle$, $\langle \mu_{2i}\rangle$, and h_j,

$$\langle S_{2i-1}\rangle = \sum_q \langle S_q\rangle \exp^{iqr_{2i-1}}, \tag{12}$$

$$\langle \mu_{2i}\rangle = \sum_q \langle \mu_q\rangle \exp^{iqr_{2i}}, \tag{13}$$

$$h_j = \sum_q h_q \exp^{iqr_j}. \tag{14}$$

Equations (10)–(14) give

$$\langle S_q \rangle = \frac{2}{3} K[J_S(q)\langle S_q \rangle + J'(q)\langle \mu_q \rangle + g\mu_B h_q], \tag{15}$$

$$\langle \mu_q \rangle = K[J_\mu(q)\langle \mu_q \rangle + J'(q)\langle S_q \rangle + g\mu_B h_q], \tag{16}$$

where $J_S(q)$, $J_\mu(q)$, and $J'(q)$ denote the Fourier components of the exchange interactions which are described by

$$J_S(q) = 2(2\alpha_S + \kappa_S \cos 2q), \tag{17}$$

$$J_\mu(q) = 2(2\alpha_\mu + \kappa_\mu \cos 2q), \tag{18}$$

$$J'(q) = 2 \cos q. \tag{19}$$

Note that the lattice constant is taken to be unity. From Eqs. (15) and (16), the wave-vector-dependent susceptibilities, which are defined by

$$\chi_S = \frac{Ng\mu_B \langle S_q \rangle}{2h_q}, \tag{20}$$

$$\chi_\mu = \frac{Ng\mu_B \langle \mu_q \rangle}{2h_q}, \tag{21}$$

are given by

$$\chi_S = \frac{N(g\mu_B)^2 K[2 + K\{J'(q) - J_\mu(q)\}]}{f(q,K)}, \tag{22}$$

$$\chi_\mu = \frac{N(g\mu_B)^2 K[3 + 2K\{J'(q) - J_S(q)\}]}{f(q,K)}, \tag{23}$$

where

$$f(q,K) = \{2KJ_S(q) - 3\}\{KJ_\mu(q) - 1\} - 2\{KJ'(q)\}^2. \tag{24}$$

The critical temperature $1/K_c$ and critical wave vector q_c are determined by the simultaneous equations

$$f(q_c,K_c) = 0, \tag{25}$$

$$\frac{\partial}{\partial q} f(q_c,K_c) = 0. \tag{26}$$

Equations (25) and (26) can be solved numerically or in some cases analytically. The results are classified into three cases: $q_c=0$, $0<q_c<\pi/2$, and $q_c=\pi/2$, which are assigned to the ferromagnetic phase, the modulated phase, and that having wave number 1/4, respectively. It should be noted that, in the ordinary ANNNI model, the critical wave number 1/4 appears only in the limit of $|J_2|/J_1 \to \infty$, i.e., the direct phase transition from the paramagnetic phase to the modulated phase with wave number 1/4 does not occur. The critical temperature for $q_c=\pi/2$ is given by

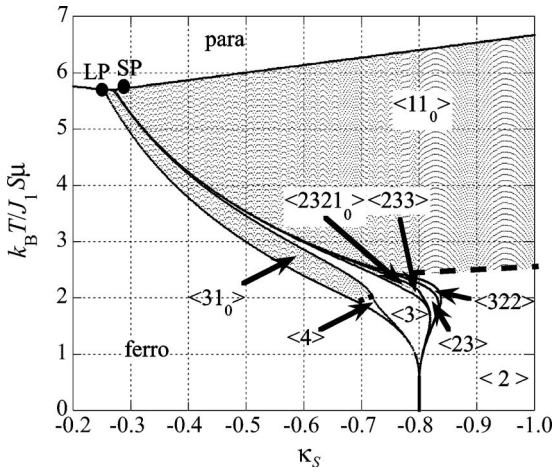

FIG. 2. Magnetic phase diagram for case 1.

$$\frac{1}{K_c} = \max\left(\frac{4(2\alpha_S - \kappa_S)}{3}, 2(2\alpha_\mu - \kappa_\mu)\right). \tag{27}$$

Equation (27) suggests the possibility that with the change of interaction ratio the slope of the linear phase boundary between the paramagnetic phase and wave number 1/4 phase may change from one to the other. This will be shown in Sec. II B.

B. Magnetic phase diagrams

In order to discuss the spin-mixing effects, we compare the results obtained for the following three cases of interaction strength: case 1 $J_0/J_1=J_0'/J_1=1$, $J_2=J_2'$; case 2 $J_0S^2/J_1S\mu=J_0'\mu^2/J_1S\mu=1$, $J_2S^2=J_2'\mu^2$; case 3 $J_0/J_1=J_0'/J_1=1$, $J_2S^2=J_2'\mu^2$.

In case 1, all exchange interactions have the same strength. Therefore, the difference of the spin value directly affects the strength of interaction energy (i.e., energy effect) between respective spin pairs. In case 2, all interaction energies between respective spin pairs have the same strength. Therefore, we can see the effect of the difference of the number of allowed spin states or spin degrees of freedom (i.e., entropy effect). Case 3 is the hybridization of cases 1 and 2.

Case 1. For this case, we took the interaction ratios defined in Eq. (5) as $\alpha_S/2=2\alpha_\mu=1$, $\kappa_S/2=2\kappa_\mu$, and performed the numerical calculation by changing the value of κ_S. The magnetic phase diagram calculated for case 1 is shown in Fig. 2. The symbols $\langle n_1 n_2 \ldots \rangle$ correspond to the modulated phases starting with an S layer, whose fundamental periods consist of successive n_1 layers, which have the same direction of magnetization, and the following n_2 layers, which have the opposite direction to the previous one, and so on. In addition, "1_0" represents a paramagnetic layer. For example, schematic spin configurations of $\langle 2 \rangle$, $\langle 31_0 \rangle$, $\langle 11_0 \rangle$, and $\langle 2321_0 \rangle$ are shown in Fig. 3, in which the direction and the length of the bars depict the orientation and magnitude of layer magnetization. In Fig. 2, the PDP phases are shown as hatched areas, and the ferromagnetic and paramagnetic phases are denoted by "ferro" and "para," respectively. The

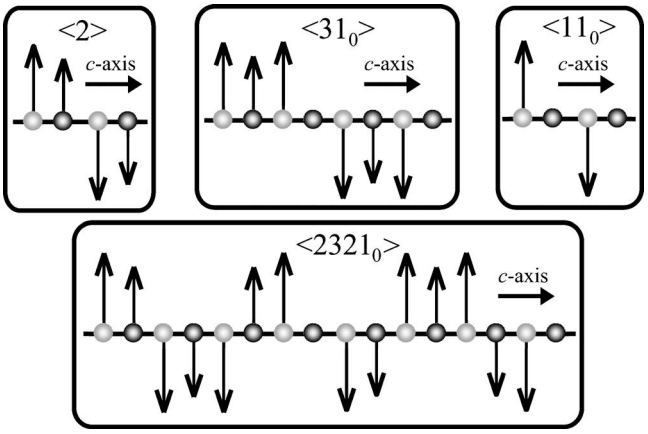

FIG. 3. Schematic spin configurations of $\langle 31_0\rangle$, $\langle 11_0\rangle$, and $\langle 2321_0\rangle$. The direction and length of the bars depict the layer magnetization of each layer. The white and black balls correspond to a S and μ layers, respectively.

point where ferromagnetic, paramagnetic, and modulated phases coexist, is designated as "LP" (Lifshitz point). Another special point is shown as "SP" (saturated point), where the critical wave number saturates to 1/4 with decreasing κ_1 (<0).

There are three PDPs having periods $\langle 31_0\rangle$, $\langle 2321_0\rangle$, and $\langle 11_0\rangle$. All these PDPs include paramagnetic μ layers. In case 1, the interaction energy related to the larger spin S is larger than that of the smaller spin μ. Then, with the decrease of temperature, the ordering of the S layer can be more easily established than that of the μ layer resulting in a PDP which includes paramagnetic μ layers.

Case 2. For this case, we took the interaction ratios defined in Eq. (5) as $\alpha_S=\alpha_\mu=1$, $\kappa_S=\kappa_\mu$, and performed the numerical calculation by changing the value of κ_S. The phase diagram is shown in Fig. 4. We note that there appear three PDPs as in Fig. 2. The apparent difference between in Figs. 2 and 4 is that the modulated PDPs are $\langle 31_0\rangle$, $\langle 2321_0\rangle$, and $\langle 11_0\rangle$ in Fig. 2 but $\langle 1_03\rangle$, $\langle 1_0232\rangle$, and $\langle 1_01\rangle$ in Fig. 4, respectively. Namely, in contrast to case 1, the PDPs in Fig. 4 include paramagnetic S layers. In case 2, the interaction energy between respective spin pairs is the same, so the entropy is the dominant term in free energy for determining stable spin states. Then with increase of the temperature, the layer including the larger spin S becomes paramagnetic more easily than that with the smaller spin.

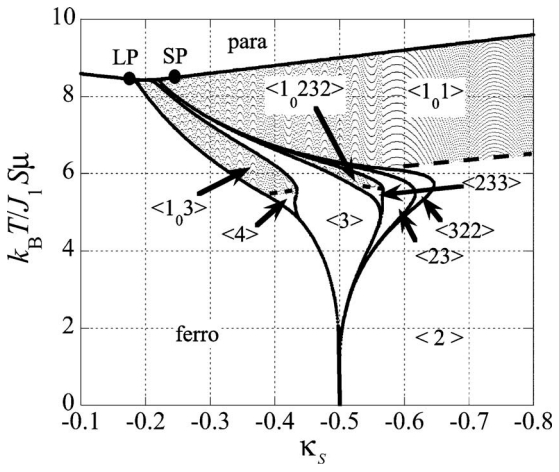

FIG. 4. Magnetic phase diagram for case 2.

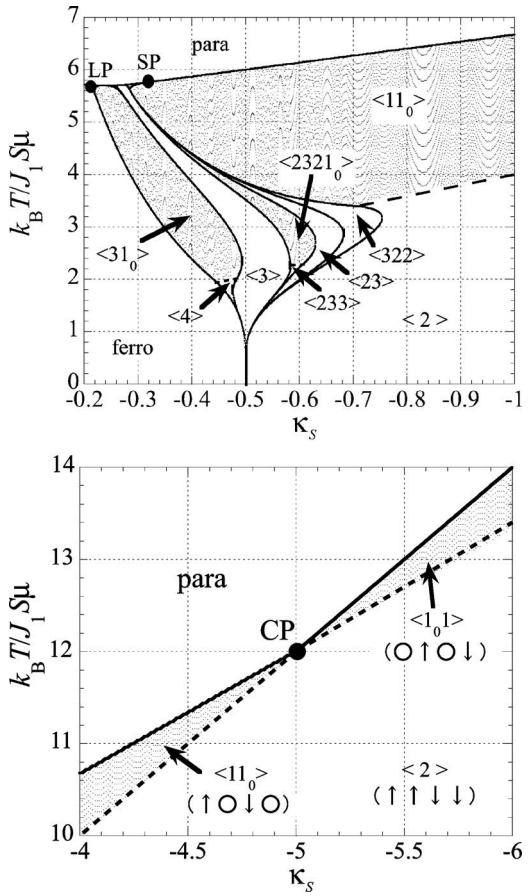

FIG. 5. Magnetic phase diagram for case 3.

Case 3. For this case, we took the interaction ratios defined in Eq. (5) as $\alpha_S/2=2\alpha_\mu=1$, $\kappa_S=\kappa_\mu$, and performed the numerical calculation by changing the value of κ_S. The phase diagram is shown in Fig. 5(a). It resembles Fig. 2, but the extended phase diagram [Fig. 5(b)] shows a characteristic difference from Fig. 2. In contrast to Fig. 2, the stable temperature range of the $\langle 11_0\rangle$ PDP phase becomes narrow with decreasing κ_S (<0), and finally vanishes at $\kappa_S=-5$. With further decrease of κ_S, there appears a new PDP of $\langle 1_01\rangle$ for $\kappa_S<-5$. That is to say, the crossover phenomenon between the $\langle 11_0\rangle$ PDP and $\langle 1_01\rangle$ PDP occurs at $\kappa_S=-5$ [crossover point (CP)].

To our knowledge, the crossover phenomenon between two different PDPs is detected here for the first time. Generally, MFA results do not accurately describe critical temperatures because of neglecting spin correlations and fluctuations. Therefore, it has to be checked that the CP can be reproduced by more accurate methods, for example MC simulation. However, even if the crossover phenomenon can be reproduced by MC simulation, it is expected that the interaction strength and critical temperature for CP quantitatively differ from those obtained by the MFA. To overcome

this problem, before performing the MC simulation, we find the main factor leading to the CP by using the MFA.

C. Simple analysis of the crossover phenomenon

We give a simple argument on the occurrence of the crossover between $\langle 11_0 \rangle$ and $\langle 1_0 1 \rangle$ PDPs and find a guide to estimate the CP which will aid the MC simulation in the next section. In the vicinity of the CP, the NNN interactions J_2 and J_2' are dominant in the ordering of the system. It is therefore reasonable to assume $\langle S_{4i-3} \rangle = -\langle S_{4i-1} \rangle \equiv \langle S \rangle$ and $\langle \mu_{4i-2} \rangle = -\langle \mu_{4i} \rangle \equiv \langle \mu \rangle$. Under this assumption, we can obtain thermal averages of magnetizations from Eqs. (6) and (7),

$$\langle S \rangle = \frac{2 \sinh KH_S}{1 + 2 \cosh KH_S}, \tag{28}$$

$$\langle \mu \rangle = \tanh KH_\mu, \tag{29}$$

where

$$H_S = \langle S \rangle (4\alpha_S - 2\kappa_S), \tag{30}$$

$$H_\mu = \langle \mu \rangle (4\alpha_\mu - 2\kappa_\mu), \tag{31}$$

and from Eqs. (5) and (9)

$$KH_S = \frac{\langle S \rangle (4J_0 S^2 - 2J_2 S^2)}{k_B T}, \tag{32}$$

$$KH_\mu = \frac{\langle \mu \rangle (4J_0' \mu^2 - 2J_2' \mu^2)}{k_B T}. \tag{33}$$

Equations (28), (29), (32), and (33) imply that in the vicinity of the CP the mixed-spin ANNNI model is divided into two independent Ising models with spin S and spin μ, respectively. Thus the critical temperatures of these systems can be separately obtained as follows:

$$k_B T_c^S = \frac{2}{3}(4J_0 - 2J_2), \tag{34}$$

$$k_B T_c^\mu = 4J_0' - 2J_2'. \tag{35}$$

For interaction ratios $\alpha_S = 2$ and $\alpha_\mu = 0.5$, i.e., the condition of case 3, the $2J_2/J_0 \equiv \tilde{\kappa}_S$ dependencies of these critical temperatures are shown in Fig. 6. We can see that T_c^μ increases more quickly than T_c^S with decreasing $\tilde{\kappa}_S$ (<0). It should be noted that a crossover occurs at $\tilde{\kappa}_S = -5$ and $2k_B T_c^S/J_0 = 2k_B T_c^\mu/J_0 = 12$, which are consistent with the volues obtained in Fig. 5(b) since $J_0/2 = J_1 S\mu$ in the present case. We see that the NN interlayer interactions J_1 for each layer cancel out between the upper layer and lower layer and the NNN interlayer interactions J_2 and J_2' are intrinsic for the occurrence of the crossover phenomenon. This physical picture for the crossover phenomenon is very useful in the following MC simulation.

III. MONTE CARLO SIMULATION

In this section, we perform a MC simulation focused on the examination and confirmation of the crossover phenomenon between $\langle 11_0 \rangle$ and $\langle 1_0 1 \rangle$ PDPs. Following the scheme of Sec. II C, first we perform MC simulations for two independent Ising models with spin $S=1$ and spin $\mu=1/2$, respectively. Next, we introduce and study their coupled version, i.e., the mixed-spin ANNNI model.

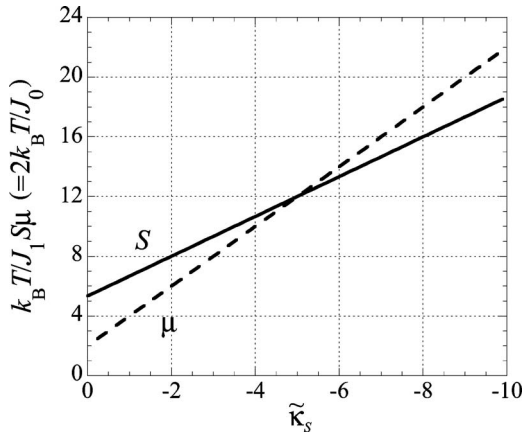

FIG. 6. MFA results of the critical temperatures of Ising models with spin $S=1$ (solid line) and spin $\mu=1/2$ (broken line). The renormalization by J_0 is for comparison with the results of Monte Carlo simulation which are shown in Fig. 7.

A. Two independent Ising models

Under the condition of $J_1=0$, the mixed-spin ANNNI Hamiltonian is divided into the following two independent Ising Hamiltonians:

$$\mathcal{H}_S = -J_0 S^2 \sum_{\langle ij \rangle} S_i S_j - J_2 S^2 \sum_{\langle ij \rangle} S_i S_j, \tag{36}$$

$$\mathcal{H}_\mu = -J_0' \mu^2 \sum_{\langle ij \rangle} \mu_i \mu_j - J_2' \mu^2 \sum_{\langle ij \rangle} \mu_i \mu_j, \tag{37}$$

where $\mathcal{H}_S$ ($\mathcal{H}_\mu$) is the $S=1$ ($\mu=1/2$) Ising model with the ferromagnetic intralayer interaction J_0 (J_0') and the antiferromagnetic NN interlayer interaction J_2 (J_2').

We used the standard importance sampling method with the Metropolis algorithm on an $L \times L \times L$ simple cubic lattice ($L=40$) with periodic boundary conditions along the three axes. The result for the initial 10^4 Monte Carlo steps per spin (MCS) at each temperature was disregarded and the result for the subsequent 10^4 MCS was used for calculation of physical quantities. The results during the latter 10^4 MCS are divided into ten samples in order to estimate the standard deviation. The last spin configuration of each temperature is employed as an input for calculation at the next temperature. Starting from very low temperature, we calculated the specific heat as the fluctuation in the internal energy. The critical temperatures were determined from the maximum of the specific-heat curve. The strength of the intralayer interactions was fixed as $J_0 = J_0'$ as in case 3 and Sec. II C.

The $\tilde{\kappa}_S$ dependence of the critical temperatures is shown in Fig. 7(a) for the case of $J_2 S^2 = J_2' \mu^2$ in order to compare with the MFA result of Fig. 6. Both critical temperatures for the $S=1$ and $\mu=1/2$ Ising models increase with decreasing

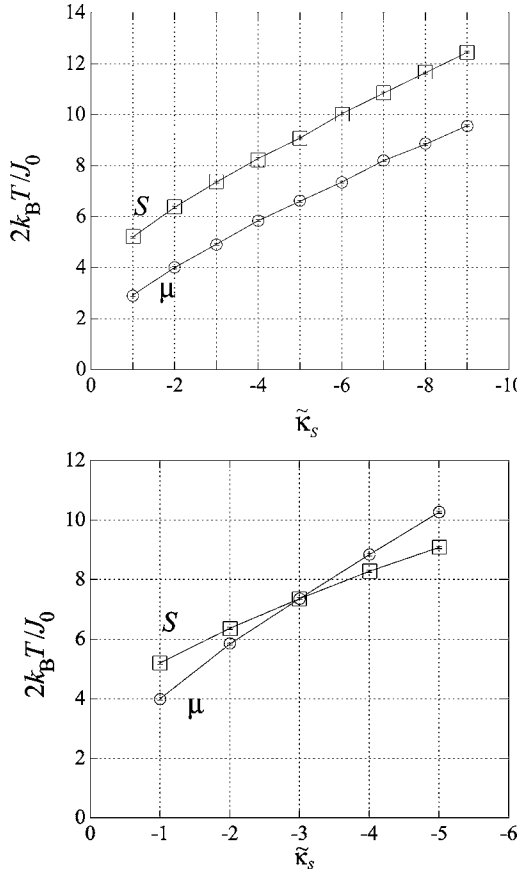

FIG. 7. Monte Carlo results of the critical temperatures of two independent Ising models with spin $S=1$ (squares) and spin $\mu=1/2$ (circles) against $\tilde{\kappa}_S=2J_2/J_0$ for (a) $J_2S^2=J_2'\mu^2$ and (b) $2J_2S^2=J_2'\mu^2$.

$\tilde{\kappa}_S$. The difference between the two critical temperatures, however, extends with further decreasing of $\tilde{\kappa}_S$, and the crossover is not observed. This means that in practice the parameter used in the MFA calculation cannot produce the crossover phenomenon. In order to confirm the crossover, we performed further MC simulations by changing the ratio J_2'/J_2. In Fig. 7(b), we show the MC result for $2J_2'S^2=J_2\mu^2$. In this case, we can really observe the crossover between two critical temperatures at $\tilde{\kappa}_S=-3.0$ and $2k_BT/J_0=7.2$.

In the MFA which neglects spin correlations, the field interacting with a spin is simply approximated as proportional to the thermal expectation value of the neighboring spin, and then the NN interlayer interaction has been perfectly canceled out at the CP. However, even in a region of strong frustration like the CP, correlations between frustrated spins should affect the frustration effect, spin stability, and finally the location of the CP. In the next section, we introduce the NN interlayer interaction and examine the crossover phenomenon of the mixed-spin ANNNI model by using MC simulation. With inclusion of the interaction J_1, there appears a strong frustration effect and we will need to reexamine and rechoose an appropriate set of values of the interactions in order to check the crossover phenomenon.

B. Monte Carlo simulation for the mixed-spin ANNNI model

In this section, we directly examine the existence of the CP in the mixed-spin ANNNI model. We used the Metropolis MC algorithm to study the difference between temperature dependences of layer magnetizations defined as follows:

$$\langle M_{S,2i-1}\rangle = \left\langle \frac{S}{L^2} \sum_{x\in S \text{ layer}} S_{2i-1,x} \right\rangle = S\langle S_{2i-1}\rangle, \tag{38}$$

$$\langle M_{\mu,2i}\rangle = \left\langle \frac{\mu}{L^2} \sum_{x\in \mu \text{ layer}} \mu_{2i,x} \right\rangle = \mu\langle \mu_{2i}\rangle. \tag{39}$$

In Eqs. (38) and (39), the summations run over the spins placed on the $(2i-1)$th $(2i$th$)$ S layer (μ layer). From very low temperature, we calculated the layer magnetizations in the same heating procedure as that explained and used in Sec. III A.

In the calculation of the temperature dependence of the layer magnetizations, the period-four modulation $\langle 2\rangle$ was set as the initial spin configuration on the lattice, which has sufficiently large size $(L\times L\times L_z)=(60\times 60\times 40)$. After discarding the first 10^5 MCS for equilibration at each temperature, thermal averages are calculated using the subsequent 10^5 MCS. The error bars were calculated by taking all the results for the latter 10^5 MCS and grouping them into 10^2 samples to calculate a thermal average and a standard deviation. Figure 8(a) shows the temperature dependences of the layer-magnetizations for $\kappa_S=-2$ with $1.7J_2S^2=J_2'\mu^2$. In the temperature range between $k_BT/J_1S\mu=5.4$ and 6.4, $\langle M_{\mu,2}\rangle \simeq 0$ and $\langle M_{\mu,4}\rangle \simeq 0$ while $\langle M_{S,1}\rangle$ and $\langle M_{S,3}\rangle$ remain finite.

In order to see the system size dependence of the layer magnetizations, we performed MC simulation at a fixed temperature for several systems of size $L=30$, 40, 48, 56, and 60 with fixed $L_z=40$. For each simulation, the result of the initial 10^6 MCS was disregarded and the results of the subsequent 10^6 MCS were devided into 10^3 samples to calculate a thermal average and a standard deviation. The least-square fitting plots of $\langle M_{S,1}\rangle$ and $\langle M_{\mu,2}\rangle$ against $1/L$ at $k_BT/J_1S\mu=5.8$ are shown in Fig. 8(b). This figure shows that the finite-size effect of the lattice causes a finite $\langle M_{\mu,2}\rangle$, and $\langle M_{\mu,2}\rangle$ completely vanishes in the limit $L\to\infty$. (Note that the order parameters $\langle M_{S,2i-1}\rangle$ and $\langle M_{\mu,2i}\rangle$ will have the same character as in a two-dimensional system. The size dependence of $\langle M_{S,2i}\rangle$ and $\langle M_{\mu,2i-1}\rangle$ therefore should obey the $1/L$ variation.) From Fig. 8, we conclude that the $\langle 11_0\rangle$ PDP exists at $\kappa_S=-2.0$.

On the other hand, the layer magnetizations for $\kappa_S=-15$ with $1.7J_2S^2=J_2'\mu^2$ are shown in Fig. 9 as functions of temperature and $1/L$. The details of these simulation are the same as mentioned above. Figure 9(a) shows $\langle M_{S,1}\rangle \simeq 0$ and $\langle M_{S,3}\rangle \simeq 0$ while $\langle M_{\mu,2}\rangle \neq 0$ and $\langle M_{\mu,4}\rangle \neq 0$ between $k_BT/J_1S\mu=17$ and 17.8 in contrast to Fig. 8(a). In addition, Fig. 9(b) shows $\langle M_{S,1}\rangle=0$ at the thermodynamic limit. Accordingly, the $\langle 1_01\rangle$ PDP is stable at $\kappa_S=-15$.

From Figs. 8 and 9 we can conclude that the $\langle 11_0\rangle$ and $\langle 1_01\rangle$ phases are stabilized at $\kappa_S=-2$ and -15, respectively. These results imply the existence of a CP between $\kappa_S=-2$

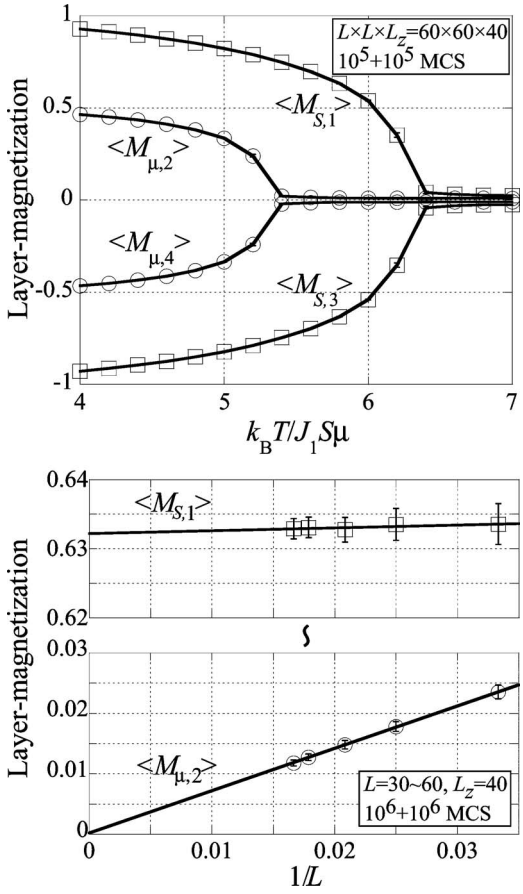

FIG. 8. Layer magnetizations $\langle M_S\rangle$ (squares) and $\langle M_\mu\rangle$ (circles) on $\kappa_S=-2$ against (a) the temperature variation for $(L,L,L_z)=(60,60,40)$ and (b) the L variation at $k_BT/J_1S\mu=5.8$.

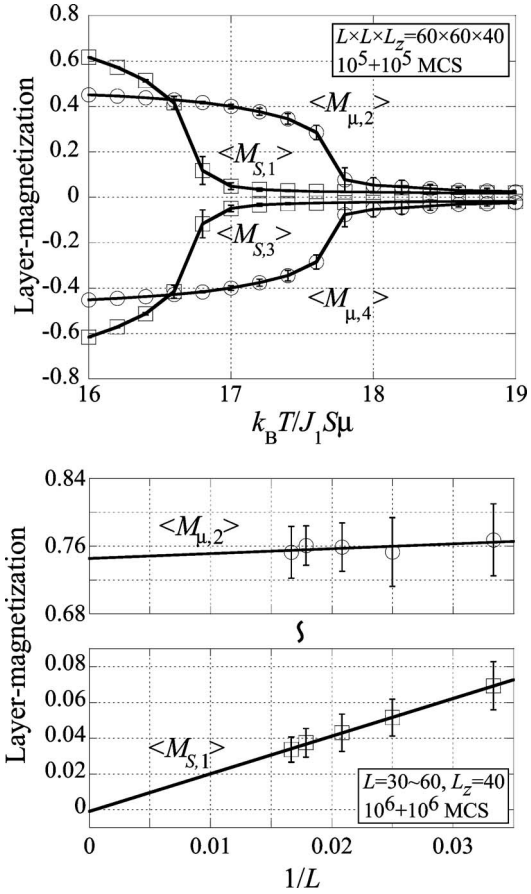

FIG. 9. Layer magnetizations $\langle M_S\rangle$ (squares) and $\langle M_\mu\rangle$ (circles) at $\kappa_S=-15$ against (a) the temperature variation for $(L,L,L_z)=(60,60,40)$ and (b) the linear L variation at $k_BT/J_1S\mu=17.2$.

and −15. These MC results are qualitatively consistent with those obtained from the MFA calculations.

IV. CONCLUDING REMARKS

We have studied the partially disordered phase of the $S=1$ and $\mu=1/2$ mixed-spin ANNNI model. By using the MFA, we have discussed the following three cases changing the strength of competing interactions: case 1, $J_0=J_0'$ and $J_2=J_2'$; case 2, $J_0S^2=J_0'\mu^2$ and $J_2S^2=J_2'\mu^2$; and case 3, $J_0=J_0'$ and $J_2S^2=J_2'\mu^2$. In case 1, the difference between the magnitudes of spin S and of spin μ mainly affected the internal energy and the energy gain determining the structure of spin ordering. As a result, we observed a PDP composed of paramagnetic μ layers. In case 2, the entropy gain of the larger spin S reduced the free energy. Then, in contrast to case 1, we found PDP including the paramagnetic S layers. In case 3, which is the hybridization of cases 1 and 2, we observed a crossover phenomenon between two different types of PDP mentioned above at their crossover point.

By simple MFA calculation, we discussed the physical background of the appearance of the crossover phenomenon. Referring to this MFA consideration, first we performed MC simulations for the two independent spin-S and spin-μ Ising models, respectively. Next, we introduced their coupling (NN interlayer interaction) in the calculation, and practically confirmed the appearance of a crossover between the PDP including paramagnetic spin-μ layers ($\langle 11_0\rangle$) and paramagnetic spin-S layers ($\langle 1_01\rangle$), respectively.

In this paper, we have systematically studied the mixed-spin ANNNI model by choosing appropriate sets of values of the interactions. The present model is an extended version of the previous ordinary ANNNI model. Then, by taking an

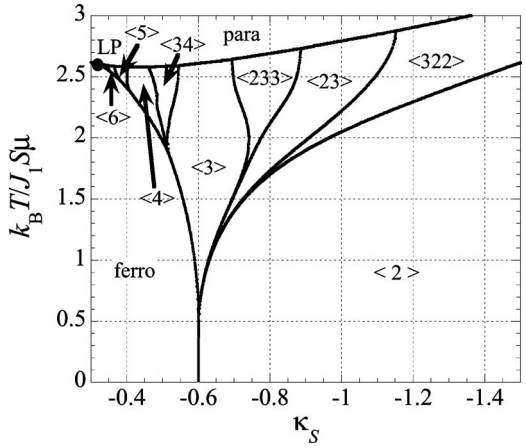

FIG. 10. Magnetic phase diagram for case 4.

appropriate set of values of parameters, we can reproduce the phase diagram which resembles the previous ordinary ANNNI model showing no PDP. Actually, for example, we performed the MFA calculation for the set of interactions $\alpha_S=3$, $\alpha_\mu=2$, and $2\kappa_S=3\kappa_\mu$ (case 4), in which the strength of the interactions is fixed to the inverse ratio of critical temperatures, i.e., $S^2/S(S+1):\mu^2/\mu(\mu+1)=3:2$. The magnetic phase diagram obtained is shown in Fig. 10. In Fig. 10, the PDP does not appear and the SP exists only in the limit of $\kappa_S\rightarrow-\infty$. We note that this phase diagram is almost the same as that of the ordinary ANNNI model calculated by the MFA, except for a slight difference in the periods of modulated phases. This difference is due to the restriction of N. In the present calculation for $N<16$, phases corresponding to $q=0$ and $\pi/8\leqslant q\leqslant\pi/2$ can be taken into account. For higher values of N, complex structures with longer periodicities will appear in the phase diagram. These structures, however, are not stable except within an extremely narrow temperature range in the phase diagram, and so no additional significant insight can be achieved by extending the numerical calculation to such higher values of N.[9]

In the present paper, we focused our attention on the investigation and confirmation of the appearance of PDSs and their crossover behavior by using a rather simple molecular field and Monte Carlo calculation. Detailed analysis of the critical properties of the phase transition between the completely paramagnetic state and the PDS particularly around the crossover point will be very interesting future work to be studied. Finally, it will also be an interesting future problem to extend the present calculation to larger-spin cases and/or mixed-spin systems having other combinations of spin values.

[1] T. Kaneyoshi and M. Jaščur, J. Phys.: Condens. Matter **5**, 3253 (1993); T. Kaneyoshi, Physica B **210**, 210 (1995).
[2] S. I. Ohkoshi, Y. Abe, A. Fujishima, and K. Hashimoto, Phys. Rev. Lett. **82**, 1285 (1999).
[3] A. Bobak, J. Dely, and T. Balcerzak, Czech. J. Phys. **54**, D523 (2004). See also A. Bobak, F. O. Abubrig, and T. Balcerzak, Phys. Rev. B **68**, 224405 (2003).
[4] G. H. Wannier, Phys. Rev. **79**, 357 (1950).
[5] M. Mekata, J. Phys. Soc. Jpn. **42**, 76 (1977).
[6] S. Fujiki, K. Shutoh, Y. Abe, and S. Katsura, J. Phys. Soc. Jpn. **52**, 1531 (1983).
[7] M. Mekata and K. Adachi, J. Phys. Soc. Jpn. **44**, 806 (1978).
[8] T. Horiguchi, O. Nagai, S. Miyashita, Y. Miyatake, and Y. Seo, J. Phys. Soc. Jpn. **61**, 3114 (1992).
[9] P. Bak and J. von Boehm, Phys. Rev. B **21**, 5297 (1980).
[10] J. Rossat-Mignod, P. Burlet, H. Bartholin, O. Vogt, and R. Lagnier, J. Phys. C **13**, 6381 (1980); J. Rossat-Mignod, P. Burlet, J. Villain, H. Bartholin, Wang Tcheng-Si, D. Florence, and O. Vogt, Phys. Rev. B **16**, 440 (1977).
[11] Y. Muraoka, T. Kasama, T. Shimamoto, K. Okada, and T. Idogaki, Phys. Rev. B **66**, 064427 (2002).
[12] T. Kasama, T. Shimamoto, Y. Muraoka, K. Okada, and T. Idogaki, Physica B **329-333**, 1061 (2003); T. Kasama, Y. Muraoka, and T. Idogaki, J. Magn. Magn. Mater. **272-276**, Suppl. 1, E995 (2004).